Acousto-optic low-frequency shifter

M. G. Gazalet, M. Ravez, F. Haine, C. Bruneel, and E. Bridoux

Here a large deflection angle, low optical frequency-shift acousto-optic device is presented. This is realized by two successive acousto-optic interactions in the same cell. The relevant parameters of operation are analyzed in detail. A practical case with paratellurite material is then considered. Results from numerical computations leading to practical design parameters are given and compared with experimental ones.

Key words: Acousto-optics, modulation, frequency shifter.

1. Introduction

The low-frequency shift of a monochromatic laser beam may sometimes be required, for example, in optical gyroscope applications.[1,2] Typically in the phase-nulling method,[3] a frequency shift of 1 Hz corresponds to an angular velocity of approximately 1°/h.[4,5] We can consider that few megahertz frequency shifts[3] are required with an absolute precision of ~1 Hz.

A convenient method to shift the optical frequency is the acousto-optic interaction.[6–8] In an acousto-optic device, it is well known that the angular deflection is proportional to the acoustic frequency[9] and that the frequency shift of the diffracted optical beam is equal to the acoustic frequency. It is therefore clear that, when low-frequency shifts are required, the angular deflection will be so small that a small fraction of the undiffracted (frequency-unshifted) light beam will be diffused in the direction of the diffracted beam. When this light is detected by a photodiode, a spurious signal at acoustic frequency will occur because of heterodyne effects.

A way to avoid this phenomenon is presented here. It consists of two successive acousto-optic diffractions with two high, nearly equal, acoustic frequencies. The two angular deflections θ_1 and θ_2 are in the same circular direction, but the two acoustic waves are generated in opposite directions (by using two transducers) such that the overall frequency shift is equal to the difference between the two acoustic frequencies f_1, f_2,[2] shown in Fig. 1. A paratellurite cell is analyzed and a practical realization is presented.

The authors are with the Département d'Opto Acousto Electronique, Institut d'Electronique et de Microélectronique du Nord (Unité Mixte de Recherche Centre National de la Recherche Scientifique 9229), Université de Valenciennes, BP311 59304, Valenciennes Cedex, France.

Received 9 July 1992; revised manuscript received 26 January 1993.

0003-6935/94/071293-06$06.00/0.

2. Design Considerations

The proposed acousto-optic cell is made of paratellurite material (TeO_2) because of the existence of a shear acoustic wave propagating along the (110) crystallographic axis enjoying a very low velocity (v = 615 m/s).[11] This results in an exceptionally high figure of merit ($M_2 = 1.2 \times 10^{-12}$ s^3/kg)[12] and in high diffraction angles θ:

$$\theta = \lambda f/v, \tag{1}$$

where λ is the optical wavelength in vacuum and f is the acoustic frequency. Experimental studies for the acoustic wave attenuation in paratellurite are also available.[13]

In this paper we present the basic design considerations. First, the propagation of both acoustical and optical waves in paratellurite shows high anisotropic effects that must be considered. These are reported in Subsection 2.A. The choice between different configurations will be made on the basis of the minimization of spurious effects such as second-order rediffraction and optical activity consequences, described in Subsections 2.B and 2.C, respectively.

Particular applications generally require a fixed direction for the output beam.[14] This may be achieved with a method quite similar to that proposed by Cheng and Tsai,[15] by simultaneously tuning the two frequencies f_1 and f_2 such that their sum $f_1 + f_2$ remains approximately constant. This is discussed

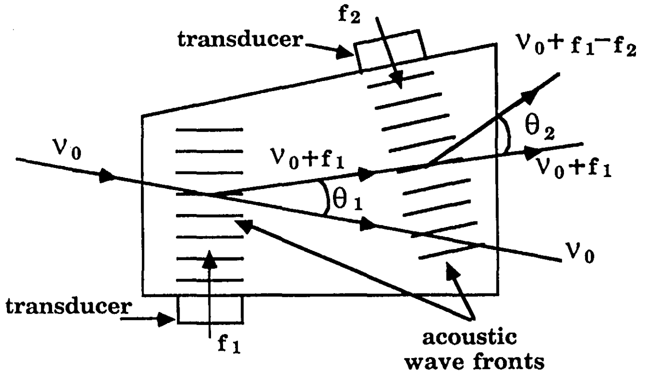

Fig. 1. Geometrical configuration of the double acousto-optic interaction; ν_0 is the laser frequency and f_1 and f_2 are the two acoustic frequencies.

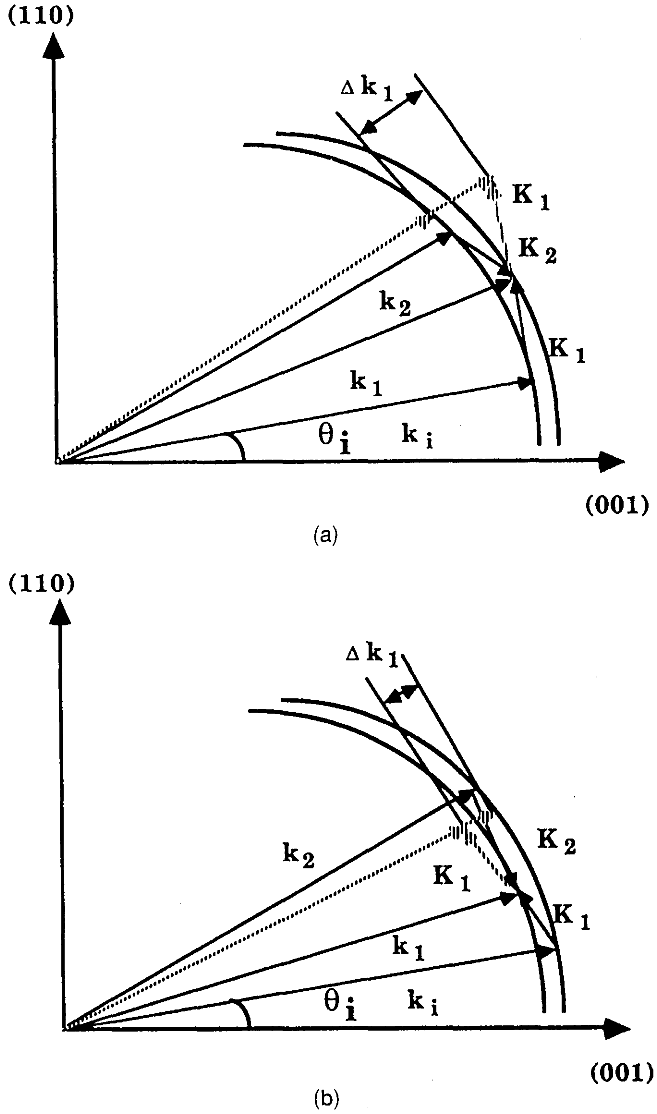

Fig. 2. Interaction wave-vector diagram: (a) IEI, (b) EIE. The dotted lines represent the second-order rediffraction related to the first interaction.

in Subsection 2.D in relation to the phenomena described in the other sections.

A. Effect of the Optical and Acoustical Anisotropy

The TeO_2 material is optically positive uniaxial.[16] The acousto-optic diffraction using the slow shear wave described above is associated with a change in polarization of the optical wave. We then have to consider two wave-vector configurations in the $(1\bar{1}0)$ plane for the double interaction, according to the polarization of the incident optical wave.

First, the incident light is ordinarily polarized (wave vector lying on the internal surface wave). In accordance with the locus of the optical wave vectors for incident first and second diffracted waves, this will be denoted internal–external–internal (IEI) interaction. The wave-vector diagram for this type of successive interaction is shown in Fig. 2(a). Similarly, if the incident light is extraordinarily polarized, the interaction will be denoted external–internal–external (EIE), shown in Fig. 2(b). On both figures **K** stands for acoustical wave vectors whereas **k** stands for the optical ones. Index i refers to the incident wave vector, and indices 1 and 2 refer to the interaction with first and second acoustic waves, respectively.

The parartellurite crystal shows exceptionally high anisotropic effects for an acoustic wave propagating in direction near the (110) crystallographic axis.[11] That is, the slowness $s = 1/v$ decreases rapidly with the wave direction. This leads to a variation in the magnitude of the acoustic wave vector with propagation direction (i.e., with the angle θ_a between the acoustic wave vector and the 110 direction) for a fixed acoustic frequency. This must be taken into account for the determination of the geometrical configuration for synchronous acousto-optic interaction. This also leads to a high obliquity δ for the acoustic wave that may reach more than 50° (Ref. 17). This will considerably increase the dimensions of the acousto-optic crystal. Finally, this leads to a decrease in the figure of merit M_2 proportional to the cube of the slowness. Figure 3 shows the relative variations of the figure of merit versus acoustic angle θ_a:

$$M_{2\text{rel}} = \frac{M_2(\theta_a)}{M_2(0)}. \tag{2}$$

B. Second-Order Rediffraction

Because a high efficiency is required for both interactions, a dip may occur in the acoustic frequency bandwidth.[18,19] This is due to second-order rediffraction with either acoustic wave. In our device the first acoustic wave is responsible for a second diffracted order propagating in a direction close to the final frequency-shifted optical wave. For both IEI and EIE configurations, this side effect will therefore be more troublesome for the first acousto-optic interaction than for the second one.

To reduce the magnitude of this rediffraction, we choose the interaction geometry such that the unwanted order is affected by a large phase mismatch

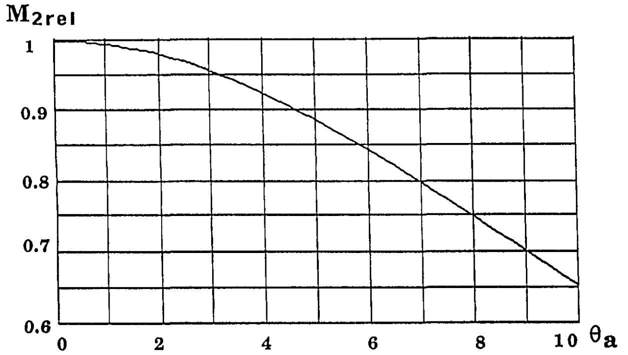

Fig. 3. Variations of figure of merit (relative to its maximal value) M_{2rel} versus acoustical direction θ_a [in degrees, measured from the 110 direction in the $(1\bar{1}0)$ plane].

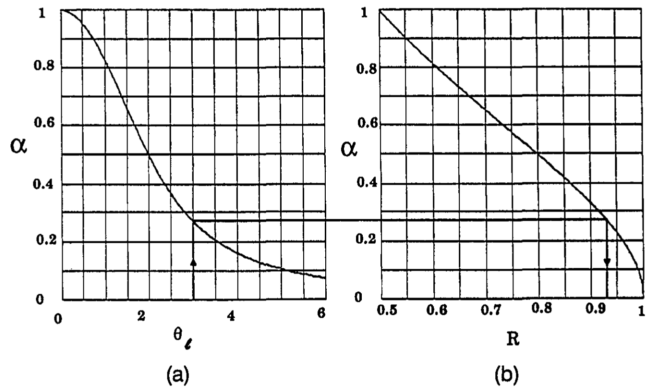

Fig. 4. Variations of (a) elliptical ratio α versus light angular direction θ_l (in degrees) for an optical wavelength $\lambda = 0.8$ μm, (b) coupling factor R (abscissa) versus elliptical ratio α (ordinate).

$\Delta\varphi_1$. The phase mismatch is defined as

$$\Delta\varphi = W \cdot \Delta\mathbf{k}, \tag{3}$$

where W is the transducer width in the direction of light propagation and $\Delta\mathbf{k}$ is the asynchronism vector as defined in Ref. 20.

The asynchronism wave vector $\Delta\mathbf{k}_1$ corresponding to the second-order rediffraction with the first acoustic wave is shown by dotted lines in Fig. 2. It is simply the difference between the vectorial sum $\mathbf{k}_1 + 2\mathbf{K}_1$ and the eigenwave vector propagating in the same direction with the proper polarization state. It is then obvious, from Figs. 2(a) and 2(b) that this asynchronism wave vector $\Delta\mathbf{k}_1$ is larger for the IEI configuration than for the EIE one. The first configuration will therefore be favorable from second-order rediffraction considerations.

C. Effects of the Optical Activity

In addition to birefringence effects, the TeO_2 also shows optical activity, especially for waves propagating close to the optical axis direction.[12,19,21] These gyrotropic effects have to be considered because (a) they will modify the wave-vector surfaces at the vicinity of the optical axis[22,23] and then affect the geometrical configuration for the interaction, and (b) the optical eigenpolarizations are no longer linear but elliptical. The ratio α of the small to large axis is shown in Fig. 4(a) as a function of θ_l, the angle between the light wave vector and the optical axis (θ_l is measured inside the crystal). If, as usual, the incident wave is linearly polarized, only a fraction of it may be coupled to the elliptically polarized propagation mode; the remainder is coupled to the other propagation mode and does not match interaction conditions. For a given α, the useful fraction reaches its maximal value $\boldsymbol{R}$ when the linear polarization is parallel to the large axis of the elliptical polarization vector. Figure 4(b) represents the R versus α evolution according to the formula

$$R = \frac{1}{1 + \alpha^2}. \tag{4}$$

For example, with an optical wavelength $\lambda = 0.8$ μm, if $\theta_l = 3°$ then this results in $\alpha = 0.28$ [Fig. 4(a)], which in turn gives $R = 0.93$ [Fig. 4(b)]. This relation may also be applied to heterodyne detection: When a linearly polarized beam beats on a photodiode with an elliptically polarized beam, the amplitude of the detected electrical signal is then decreased by the factor R with respect to the case of two beams linearly polarized in the same direction. In phase-nulling fiber-optic laser gyroapplications,[3] we are therefore interested in the highest possible values of R for the incident order $\mathbf{k}_i$ and for the frequency-shifted order $\mathbf{k}_2$.

D. Variations of the Shifted Frequency Beam Angular Deviation

In the fiber-optic gyroapplication, the output angle of the doubly diffracted light must not vary with the frequency shift $\delta f = f_1 - f_2$. That is, the overall angular deflection in any case must be equal to that with zero frequency shift, i.e.,

$$\frac{\lambda f_1}{v_1} + \frac{\lambda f_2}{v_2} = \lambda f_0\left(\frac{1}{v_1} + \frac{1}{v_2}\right),$$

where f_0 is the center frequency of each interaction and v_1, v_2 are the velocities for first and second acoustic waves, respectively.

This relation between f_1 and f_2 may be written in the parametric form

$$f_1 = f_0 + \delta f \frac{v_1}{v_1 + v_2},$$

$$f_2 = f_0 - \delta f \frac{v_2}{v_1 + v_2}. \tag{5}$$

If v_1 and v_2 are not too different one from the other, this relation will be very close to the more usual one with constant sum $f_1 + f_2$:

$$f_{1,2} = f_0 \pm \frac{\delta f}{2}. \tag{6}$$

If, for convenience, the frequencies are varied in accordance with Eq. (6) instead of the ideal Eq. (5), the variation in angular deflection with δf will be given by

$$\delta\theta = \lambda \frac{\delta f}{2}\left(\frac{1}{v_1} - \frac{1}{v_2}\right).$$

This variation will be undiscernible as long as it is small compared with the optical beam divergence λ/L, where L is the width of the light beam in the interaction plane. The acousto-optic cell may thus be driven with two acoustic waves with frequencies given by Eq. (6) as long as the condition

$$|\delta f| < \frac{v_1 v_2}{L(v_1 - v_2)} \tag{7}$$

is verified.

3. Numerical Computations

The numerical computations have been carried on for both EIE and IEI configurations. For each type, the incidence angle θ_i has been varied from 3° to 6°30′ (angle θ_i is measured inside the crystal). Lower values will reduce the R factor, whereas higher angles will require large values of θ_a and the figure of merit M_2 will be considerably reduced.

Each interaction is evaluated by the intersection of two wave-vector loci: the optical wave-vector locus (taking into account the polarization change at each acousto-optic diffraction) and the acoustic wave-vector locus for an $f_0 = 100$ MHz acoustic wave (considering acoustic velocity changes with respect to the acoustic angles θ_a).

For each interaction, the calculation results in the numerical values for the angular direction for the acoustic wave θ_a, the relative figure of merit M_2, the optical coupling factors R_i and R_2 for the incident and doubly diffracted light, respectively, the minimal transducer width $W_{\min}$ for a negligible second-order diffraction efficiency (assuming a minimal phase mismatch of 10π for the rediffraction with each acoustic wave), the maximal transducer width $W_{\max}$ for an acoustic frequency bandwidth at least equal to 10 MHz (this is calculated from the classical formulas of Ref. 9), and the product $W_{\max}M_{2\mathrm{rel}}$, because the acoustic power needed for a given efficiency will be inversely proportional to this value.[24,25] These numerical results are summarized in Tables 1 and 2 for IEI and EIE interactions, respectively.

4. Experimental Realization

A. Acousto-Optic Cell

Because the acoustic power required for a fixed interaction efficiency is inversely proportional to both the width W and the figure of merit M_2, we have to maximize the worst value of the product M_2W, i.e., $W_{\max1}M_{2\mathrm{rel}1}$ for the IEI configuration and $W_{\max2}M_{\mathrm{rel}2}$ for the EIE one.

From Tables 1 and 2, we see that the IEI configuration is more favorable from these considerations. The limitation arises from the first interaction, because the second one has a very large bandwidth as a result of nearly tangential phase matching.[26,27] Another reason for choosing the IEI configuration is the much lower value for $W_{\min1}$, because for practical values of W_1 the ratio $W_1/W_{\min1}$ will be high and therefore the second-order rediffraction by the first acoustic wave will be negligible.

For the practical realization, we have chosen the configuration with $\theta_i = 5°$ for the lost fraction of input light $1 - R$ less than 1%, together with a good value of $W_{\min1}M_{2\mathrm{rel}1}$. This corresponds to acoustic angles $\theta_{a1} = 5°21'$ and $\theta_{a2} = 11°03'$, and the corresponding obliquities δ_1 and δ_2 are 43° and 56°, respectively.

For this configuration, relation (7) shows that for $L = 240$ μm, the frequency shift must be limited to +23 MHz for no discernible variation in the output angle of the doubly diffracted light. However, larger frequency shifts may be obtained without output angle variation if the acousto-optic cell is driven with frequencies f_1 and f_2 related by Eq. (5) instead of Eq. (6).

The paratellurite crystal, with large dimensions in the direction of light propagation caused by obliquity, has been oriented with an angular tolerance of ±2 min. Both transducers are rectangular, 1.5 mm wide and 1 mm high. This height H is sufficient because of the focusing of the nearly 0.8-μm wavelength laser beam in the normal configuration described in the next subsection.

Table 1. IEI Interaction

θ_i[a]	θ_{a1}[b]	θ_{a2}[b]	$M_{2\mathrm{rel}1}$	$M_{2\mathrm{rel}2}$	R_i	R_2	$W_{\min1}$ (mm)	$W_{\min2}$ (mm)	$W_{\max1}$ (mm)	$W_{\max2}$ (mm)	$W_{\max1} \times M_{2\mathrm{rel}1}$	$W_{\max2} \times M_{2\mathrm{rel}2}$
3°	3°54′	8°35′	0.929	0.722	0.931	0.999	0.08	0.51	1.76	4.4	1.635	3.177
3°30′	4°17′	9°11′	0.915	0.693	0.959	0.9992	0.07	0.34	1.72	5.7	1.574	3.95
4°	4°39′	9°47′	0.902	0.664	0.975	0.9993	0.07	0.25	1.67	8.1	1.506	5.378
4°30′	5°0′	10°25′	0.888	0.638	0.985	0.9994	0.07	0.19	1.61	15.4	1.43	9.825
5°	5°21′	11°03′	0.873	0.604	0.99	0.9995	0.06	0.16	1.55	46.2	1.353	27.905
5°30′	5°41′	11°42′	0.859	0.575	0.994	0.9996	0.06	0.13	1.49	14.7	1.28	8.453
6°	6°0′	12°23′	0.845	0.544	0.995	0.9996	0.06	0.12	1.42	7.4	1.2	2.651
6°30′	6°19′	13°04′	0.831	0.515	0.996	0.9997	0.06	0.1	1.36	4.9	1.13	2.524

[a]θ_i is the optical incidence angle.
[b]θ_{a1} and θ_{a2} are the acoustical directions.

Table 2. EIE Interaction

θ_i[a]	θ_{a1}[b]	θ_{a2}[b]	M_{2rel1}	M_{2rel2}	R_i	R_2	W_{min1} (mm)	W_{min2} (mm)	W_{max1} (mm)	W_{max2} (mm)	$W_{max1} \times M_{2rel1}$	$W_{max2} \times M_{2rel2}$
3°	4°48′	6°09′	0.896	0.838	0.931	0.99909	0.26	0.06	2.02	1.19	1.81	0.997
3°30′	3°21′	6°27′	0.873	0.825	0.959	0.99924	0.32	0.05	2.15	1.33	1.877	1.097
4°	5°54′	6°44′	0.85	0.811	0.975	0.99937	0.43	0.05	2.31	1.27	1.964	1.03
4°30′	6°28′	7°0′	0.824	0.799	0.985	0.99947	0.68	0.05	2.53	1.21	2.085	0.967
5°	7°03′	7°15′	0.797	0.787	0.99	0.99955	1.77	0.05	2.84	1.15	2.264	1.041
5°30′	7°38′	7°30′	0.769	0.775	0.994	0.99961	2.74	0.05	3.24	1.09	2.492	0.845
6°	8°14′	7°44′	0.739	0.764	0.995	0.99967	0.74	0.04	3.85	1.04	2.845	0.795
6°30′	8°51′	7°58′	0.709	0.752	0.996	0.99971	0.42	0.04	4.86	0.99	3.446	0.745

[a] θ_i is the optical incidence angle.
[b] θ_{a1} and θ_{a2} are the acoustical directions.

B. Experimental Setup

The experimental setup is described in Fig. 5. A semiconductor laser with wavelength $\lambda \approx 0.8$ μm is used as the light source (Hitachi HLP1400). The incident light is first linearly polarized in the proper direction for IEI interaction; it then passes through an optical magnifying system as a way to match its width L and its height H' ($H' < H$) to the specified values in the interaction region in the crystal. The magnifying system is used to obtain either $L \approx 6$ mm with $H' \approx 0.5$ mm for an angular measurement purpose, configuration a), or $L \approx H' \approx 240$ μm, configuration b, which is the normal mode of operation of the frequency shifter, as described below. Then either the interaction region is imaged on a photodetector or the doubly diffracted light is focused on a CCD sensor (for the measurement of the output angle variation).

C. Experimental Results

First, we measured the acousto-optic efficiency independently for each interaction, using configuration b. A peak diffraction efficiency of ~90% has been found for each, with an electrical power of 300 and 350 mW for first and second interactions, respectively, with proper electrical matching for both transducers. That is, the overall efficiency is nearly 80%.

For this same configuration b a bandwidth of 9 MHz has been measured for the first interaction. For the second one a 54-MHz bandwidth has been found; the measurement is achieved with a first interaction driven at its fixed center frequency (100 MHz). The maximal frequency shift is therefore limited by the first-interaction bandwidth, because the frequencies f_1 and f_2 are related through Eqs. (5) or (6). Notice that an excursion of plus or minus half of the frequency bandwidth for f_1 (i.e., $|f_1 - f_0| \leq 4.5$ MHz) gives a maximal frequency shift for light of ± 9 MHz according to Eqs. (5) and of ± 9.6 MHz according to Eq. (6).

The undesirable sideband levels resulting from second-order rediffraction of the first interaction (and perhaps of the second-order diffraction of the second interaction with the residual zeroth order of the first interaction) are then measured. This can easily be done when the light is focused with a diameter of 240 μm, configuration b, because the direction of the frequency-shifted order is close to the parasitic second-order diffraction. This results in a beat at $f_1 + f_2 \approx 200$ MHz on the detector. The measurement of the amplitude of this high-frequency signal shows a very low second-order rediffraction efficiency, typically 0.02–0.03%.

The deviation of the output angle of the frequency-shifted light versus $(f_1 - f_2)$ has first been measured in configuration a when the device is driven at two frequencies, f_1 and f_2, varying according to Eq. (6). With the large value for L, the angular deviation can be measured with an accuracy of nearly ± 70 μrad, because of optical diffraction. Within this accuracy a

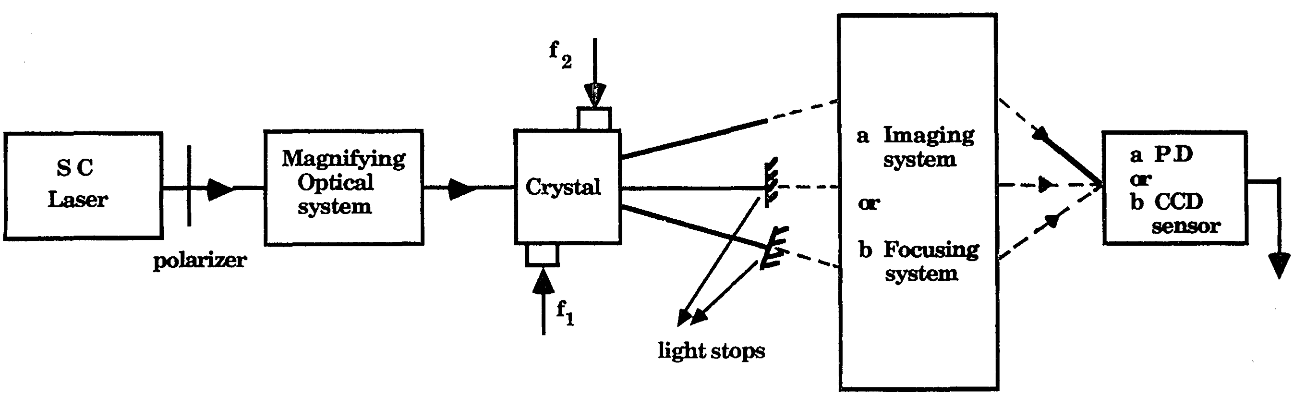

Fig. 5. Experimental setup: SC, semiconductor; PD, photodetector.

linear dependence of deflection θ with frequency shift δf has been found, and for the maximal frequency shift $\delta f_{max} = \pm 10$ MHz, an angular variation of approximately ± 700 μrad has been measured, which is in good agreement with the calculated values. The frequency f_1 is then maintained constant at 105 (95) MHz, and the frequency f_2 is varied to cancel the angular shift. This is obtained for f_2 approximately equal to 94.2 (105.8) MHz, in fair accordance with Eqs. (5).

With the magnifying system in the normal operation mode, configuration b), angular variations as larger as ± 2 mrad cannot be perceived because they are below the diffraction limitations and no distinction can be made between Eqs. (5) and (6). This has been well verified, and in practice, with $f_1 = 95$ MHz (as low as 93 MHz, respectively) without noticeable angular variation, i.e., with an acousto-optic bandwidth of 10 MHz for the first interaction, an overall frequency shift of ± 12 MHz can be reached without critical deviation of the output angle.

5. Conclusion

A practical TeO_2 low-frequency shifter using two consecutive acousto-optic interactions has been designed. The effects of optical and acoustic anisotropies as well as optical activity have been considered.

The second-order rediffraction of the first interaction has been shown to be especially inconvenient, and so it has been limited by design to very low values. Experimental verification has also been presented. Frequency shifts of ± 12 MHz can be obtained without variation in the output angle of the frequency-shifted order, which is in good agreement with the theoretical calculations.

Referencess

1. C. T. Lee, "Optical-gyroscope application of efficient crossed-channel acoustooptic devices," Appl. Phys. B **35**, 113–118 (1984).
2. P. F. Wysocki, M. J. Digonnet, and B. Y. Kim, "Broad-spectrum, wavelength-swept, erbium-doped fiber laser at 1.55 μm," Opt. Lett. **15**, 879–881 (1990).
3. R. F. Cahill and E. Udd, "Phase-nulling fiber-optic laser gyro," Opt. Lett. **4**, 93–95 (1979).
4. N. Ohgi, M. Kondoh, and M. Shimizu, "Optical fiber gyroscope with integrated optical frequency modulator," in *OFS'84*, proceedings of the Second International Conference on Optical Fiber Sensors (Papers Nachachtentechnische Geschlischaft im VDE, Stuttgart, 1984), pp. 297–300.
5. J. L. Davis and S. Ezekiel, "Techniques for shot-noise-limited inertial rotation measurement using a multiturn fiber sagnac interferometer," in *Laser Inertial Rotation Sensors*, S. Ezekiel and G. E. Knausenberger, eds., Proc. Soc. Photo-Opt. Instrum. Eng. **157**, 131–136 (1978).
6. P. Debye and F. W. Sears, "On the scattering of light by supersonic waves," Proc. Natl. Acad. Sci. USA **18**, 409–414 (1932).
7. R. Lucas and P. Biquart, "Propriétés optiques des milieux solides et liquides soumis aux vibrations élastiques ultra sonores," J. Phys. Radium **3**, 464–477 (1932).
8. A. B. Bathia and W. J. Noble, "Diffraction of light by ultrasonic waves—I General theory," Proc. R. Soc. London Ser. A **220**, 356–368 (1953).
9. I. C. Chang, "I. Acoustooptic devices and applications," IEEE Trans. Sonics Ultrason. **SU-23**, 3–22 (1976).
10. E. I. Gordon, "A review of acousto-optical deflection and modulation devices," Proc. IEEE **54**, 1391–1401 (1966).
11. Y. Ohmachi, N. Uchida, and N. Nüzeki, "Acoustic wave propagation in TeO_2 single crystal," J. Acoust. Soc. Am. **51**, 164–167 (1972).
12. T. Yano and A. Watanabe, "Acousto-optic figure of merit of TeO_2 for circularly polarized light," J. Appl. Phys. **45**, 1243–1245 (1974).
13. K. Yasutake, K. Sugiura, H. Inoue, A. Kakeuchi, M. Uemura, K. Yoshii, and H. Kawabe, "Dislocations and ultrasonic attenuation in paratellurite," Phys. Status Solidi A **125**, 489–502 (1991).
14. J. Neev and F. V. Kowalski, "Optical frequency scanning without deflection using an acoustooptic modulator," IEEE J. Quantum Electron. **26**, 1682–1685 (1990).
15. Z. Y. Cheng and C. S. Tsai, "Baseband integrated acousto-optic frequency shifter," Appl. Phys. Lett. **60**, 12–14 (1992).
16. N. Uchida, "Optical properties of single-crystal paratellurite (TeO_2)," Phys. Rev. B **4**, 3736–3745 (1971).
17. I. C. Chang, "Noncollinear acousto-optic filter with large angular aperture," Appl. Phys. Lett. **25**, 370–372 (1974).
18. A. W. Warner, D. L. White, and W. A. Bonner, "Acousto-optic light deflectors using optical activity in paratellurite," J. Appl. Phys. **43**, 4489–4495 (1972).
19. T. Yano, M. Kawabuchi, A. Fukumoto, and A. Watanabe, "TeO_2 anisotropic Bragg light deflector without midband degeneracy," Appl. Phys. Lett. **26**, 689–691 (1975).
20. J. M. Rouvaen, M. G. Ghazaleh, E. Bridoux, and R. Torguet, "On a general treatment of acousto-optic interactions in linear anisotropic crystals," J. Appl. Phys. **50**, 5472–5477 (1979).
21. A. Fukumoto, M. Kawabuchi, and H. Hayami, "Polarization considerations in the operation of two-dimensional TeO_2 abnormal Bragg deflector," Appl. Opt. **14**, 812–813 (1975).
22. M. S. Kharusi and G. W. Farnell, "Observation of optical activity in Brillouin scattering experiments," Can. J. Phys. **47**, 2719–2725 (1969).
23. R. S. Seymour, "Acoustooptic Bragg diffraction in anisotropic optically active media," Appl. Opt. **29**, 822–826 (1990).
24. T. M. Smith and A. Korpel, "Measurement of light-sound interaction efficiency in solids," IEEE J. Quantum Electron. **QE-1**, 283–284 (1965).
25. E. I. Gordon, "Figures of merit for acousto-optic deflection and modulation devices," IEEE J. Quantum Electron. **QE-2**, 104–105 (1966).
26. R. W. Dixon, "Acoustic diffraction of light in anisotropic media," IEEE J. Quantum Electron. **QE-3**, 85–93 (1967).
27. E. G. H. Lean, C. F. Quate, and H. J. Shaw, "Continuous deflection of laser beams," Appl. Phys. Lett. **10**, 48–51 (1967).